INSTITUT DE FRANCE
Académie des sciences

Comptes Rendus

Physique

Sylvestre Lacour

Astrometry of directly imaged exoplanets with optical interferometry

Published online: 25 April 2023

https://doi.org/10.5802/crphys.144

Part of Special Issue: Exoplanets

Guest editors: Anne-Marie Lagrange (LESIA, Observatoire de Paris, Université PSL, CNRS, Sorbonne Université, Sorbonne Paris Cité, 5 place Jules Janssen, 92195 Meudon, France.) and Daniel Rouan (LESIA, Observatoire de Paris, Université PSL, CNRS, Sorbonne Université, Sorbonne Paris Cité, 5 place Jules Janssen, 92195 Meudon, France.)

Les Comptes Rendus. Physique *sont membres du*
Centre Mersenne pour l'édition scientifique ouverte
www.centre-mersenne.org
e-ISSN : 1878-1535

Comptes Rendus
Physique
Published online: 25 April 2023
https://doi.org/10.5802/crphys.144

Exoplanets / *Exoplanètes*

Astrometry of directly imaged exoplanets with optical interferometry

Astrométrie des exoplanètes par interférométrie optique astronomique

Sylvestre Lacour [a]

[a] LESIA, Observatoire de Paris, Université PSL, CNRS, Université Paris Cité, Sorbonne Université, 5 place Jules Janssen, 92195 Meudon, France
E-mail: sylvestre.lacour@obspm.fr

Abstract. Optical interferometry has always been seen as a promising but difficult technique for astronomy. Until the year 2018, it was excrucially limited in sensitivity to magnitudes below 10. However, thanks to the advent of the GRAVITY instrument, fringe tracking and dual field interferometry made it possible to observe very faint target. This paper presents the different techniques used by optical interferometry to perform astrometry. It shows why dual field interferometry has become the key technique for faint companions. Taking the exemple of the HD 95086 b exoplanet, we show how dual field interferomtry can detect an exoplanet as faint as magnitude 19.5, and how its astrometry was extracted. Use this example this paper explains how and why an astrometric accuracy of 10 μas is possible, and describes the remaining biases that can hinder this measurement. Last, we conclude by presenting the orbital trajectory of 10 exoplanets in 4 systems, and conclude with the short and longer term perspectives of the technique.

Résumé. L'interférométrie aux longueurs d'ondes visibles a toujours été considérée comme une technique prometteuse mais difficile pour l'astronomie. Jusqu'à l'année 2018, sa sensibilité était limitée aux objets célestes les plus brillants, avec des magnitudes inférieures à 10. L'instrument GRAVITY, installé derrière le VLTI au Chili, a changé cela — grâce notamment à sa capacité de suivre et corriger le déplacement des franges et à son interféromètre double champ. Avec GRAVITY, l'on peut désormais observer des cibles très faibles. Cet article présente les différentes façons de faire de l'astrométrie avec un interféromètre optique. Il montre pourquoi l'interférométrie à double champ est devenue la technique clé pour les compagnons faibles. En prenant l'exemple de l'exoplanète HD 95086 b, nous montrons comment l'interférométrie à double champ peut détecter des exoplanètes aussi faibles que la magnitude 19,5. Nous expliquons également comment nous obtenons des précisions astrométriques de 10 μas, et décrivons les biais restants qui peuvent entraver la mesure. Enfin, nous terminons en présentant les orbites de 10 exoplanètes dans 4 systèmes, et concluons sur les perspectives à plus long terme de cette technique.

Keywords. Astrometry, Exoplanets, Direct detection, Interferometry, High angular resolution.

Mots-clés. Astrométrie, Exoplanètes, Détection directe, Interférométrie, Haute résolution angulaire.

Note. Follows up on a conference-debate of the French Academy of Sciences entitled "Exoplanets: the new challenges" held on 18 May 2021, visible via https://www.academie-sciences.fr/fr/Colloques-conferences-et-debats/exoplanetes.html.

Note. Fait suite à une conférence-débat de l'Académie des sciences intitulée « Exoplanètes : les nouveaux défis » tenue le 18 mai 2021, visible via https://www.academie-sciences.fr/fr/Colloques-conferences-et-debats/exoplanetes.html.

Published online: 25 April 2023

1. Introduction

Our ability to resolve details in the sky is limited in large part by the phenomenon of diffraction. When an astronomical object is observed with a telescope, the Heisenberg principle implies that the direction of the photon has a fundamental uncertainty because the photon passed through the telescope aperture and its position has thereby been constrained. More precisely, for a telescope of diameter D, the moment of the photon, $\overrightarrow{p}$ can only be known to an accuracy of $\sigma_{\overrightarrow{p}}$:

$$\sigma_{\overrightarrow{p}} = \frac{\hbar}{D}. \tag{1}$$

Since $\overrightarrow{p} = \hbar/\lambda\overrightarrow{\alpha}$, the uncertainty on the direction of the photon $\overrightarrow{\alpha}$ is limited to $\sigma_{\overrightarrow{\alpha}} = \lambda/D$. In practice, when observing at a wavelength of 2.2 µm, with an 8 meter diameter telescope, the origin of a photon can not be determined beyond a precision of 50 mas.

Several solutions have been proposed to overcome this limit. The simplest is to accumulate many photons N_p and to assume that they all come from the same direction. This improves the astrometric accuracy—the ability to locate a point source—by a factor $\sqrt{N_p}$. Significantly more complex proposals use quantum cloning or quantum squeezing, in order to improve the phase measurement of a single photon beyond the diffraction limit [1].

The technique discussed in the present article is interferometry, i.e. the combination of light collected by several telescopes. By using the Heisenberg principle on a photon that passes through a pair of telescopes, the precision on the moment of a photon is limited by $\sigma_{\overrightarrow{p}} \cdot \overrightarrow{B} = \hbar$, where $\overrightarrow{B}$ is the vector joining the two telescopes. Concretely, with 2 telescopes separated by 130 meters observing in the infrared, the origin of a photon can be determined with an accuracy of 3.4 mas, along the direction of $\overrightarrow{B}$. Of course, as with single dish telescopes, it is also possible to increase the astrometric accuracy by $\sqrt{N_p}$ on a point source.

This article describes the interferometric technique as it is presently implemented on the Very Large Telescope Interferometer (VLTI). The VLTI is an observatory at Mount Paranal in Chile. It consists of four 8 meter diameter telescopes, plus several smaller auxiliary telescopes. The light collected by these telescopes can be combined, i.a. with the GRAVITY instrument that has been installed in 2018 as a VLTI new generation instrument [2]. GRAVITY includes an original dual field combiner, which, as we will see below, enabled the observation and astrometry of exoplanets through interferometry.

Section 2 presents the principle of an astrometric measurement with an optical interferometer. Three techniques are currently in use to extract astrometry: wide field observations, single field observations and dual field observations. These are described in Section 3. The last technique is the only one which has the sensitivity to directly detect exoplanets. It is described in more details in Section 4, with its limitations in Section 5. Section 6 presents direct observations of exoplanets by our ExoGRAVITY team, and finalize this paper with perspectives and possible improvements.

2. Principle of astrometry with optical interferometry

The purpose of astrometry is to determine the position of an astronomical object. The Gaia observatory measures absolute positions of stars. It is a self-calibrated mission which yields absolute astrometric measurements with respect to sets of quasars [3]. With optical interferometry, all

measurements are done with respect to a physical length, $\overrightarrow{B}$, which denotes the separation of the two telescopes in an interferometer. $\overrightarrow{B}$ changes with time, as Earth rotates. It should therefore not be seen as a constant baseline, but as a vector that rotates relative to astronomical targets.

More precisely, in an interferometer, the origin of a photon is obtained from the difference of its optical paths through the two arms of an interferometer. This so-called OPD is obtained by the phase ϕ of the interference fringes:

$$\text{OPD modulo } (\lambda) \ = \phi \frac{\lambda}{2\pi}. \tag{2}$$

The OPD varies as a function of the wavelength. For a given measurement, at a given wavelength, the OPD is only known modulo the wavelength. The absolute optical path through each arm of the interferometer is not measured, but it includes the path of the light from the star to the telescope, and from the telescope to the detector.

Assuming that the star is located at infinity, this difference in path can be written as a scalar product between two vectors: $\overrightarrow{B}$ the vector that joins the two telescopes, and $\overrightarrow{\alpha}$ the position of the target in the sky:

$$\text{OPD} = \overrightarrow{B} \cdot \overrightarrow{\alpha}. \tag{3}$$

It is immediately observable that a phase measurement, thus the OPD, only produces a scalar product measurement: the direction of the photon can not be measured along the direction orthogonal to $\overrightarrow{B}$. If the baseline $\overrightarrow{B}$ is orthogonal to the direction of the target, then we observe an OPD which is zero. The information can however be recovered by using an interferometer with more than 2 telescopes (with several, non-aligned baselines) or by using the rotation of Earth which modifies $\overrightarrow{B}$ in the celestial reference frame.

In fact, an absolute measurement of the OPD is difficult. Therefore one rather measures a relative of optical path difference (δOPD). This works by observing two objects in two directions of the sky, $\overrightarrow{\alpha}$ and $\overrightarrow{\beta}$:

$$\delta\text{OPD} = \overrightarrow{B} \cdot (\overrightarrow{\beta} - \overrightarrow{\alpha}). \tag{4}$$

It might be useful to indicate some orders of magnitude: a modern interferometer typically measures the phase of interference fringes with an accuracy of 1°. In the near infrared, this corresponds to an accuracy of 6 nm on the δOPD. Using an interferometer with a baseline of 130 m, this corresponds to an angle of about 10 μas on sky, much below the angular resolution of the interferometer at 3.4 mas.

3. Three techniques of astrometry in optical interferometry

Astrometry with an optical interferometer aims at measuring δOPD, as shown by Equation (4). There are several ways to measure δOPD, which mostly differ by the hardware of the optical interferometer. Wide angle astrometry was implemented by the Navy Precision Optical Interferometer (NPOI) [4]. Single field astrometry was for example used by the Sydney University Stellar Interferometer (SUSI) [5]. Dual field interferometry is a technique first implemented by the GRAVITY instrument.

3.1. *Wide angle astrometry*

The aim of an interferometer is to detect and record fringes—any photons which does not contribute to the fringe pattern, contribute to the noise. At a given time, for a wavelength λ and baseline $\overrightarrow{B}$, an interferometric measurement yields 2 quantities: the phase and the amplitude of the fringes. Together, phase and amplitude yield a complex value, which is called the coherent flux, denoted **C** here.

In the case of a single object the coherent flux **C** writes:

$$\mathbf{C} = S_\alpha \exp\left(2\pi j \frac{\vec{B}\cdot\vec{\alpha}}{\lambda} + jP_{\rm atm}\right) = S_\alpha \exp\left(2\pi j \frac{\rm OPD}{\lambda} + jP_{\rm atm}\right). \quad (5)$$

S_α is the amplitude of the fringes, and of the coherent flux. On an unresolved object, the coherent flux results from the emission spectrum of the astronomical object, minus the atmospheric absorption and the loss of coherence due to instrumental effects. The atmospheric effect is represented by a chromatic piston $P_{\rm atm}$. The position of the star in the sky, $\vec{\alpha}$, introduces a linear slope on the phase of **C** as a function of $1/\lambda$.

This slope of the phase of **C** can be theoretically used to retrieve the OPD and therefore do an astrometric measurement. Unfortunately, the uncertainty on $P_{\rm atm}$ makes that impossible. The solution is for the interferometer to point two stars, one after the other, and to measure the phase of the fringes at two moments, t_1 and t_2:

$$\arg\mathbf{C}(t_1) - \arg\mathbf{C}(t_2) = 2\pi \frac{\overrightarrow{B(t_1)}\cdot\vec{\alpha} - \overrightarrow{B(t_2)}\cdot\vec{\beta}}{\lambda} \ \%\ (2\pi). \quad (6)$$

The problem of this technique is that the atmospheric piston is not the same at t_1 and t_2. A solution consists in averaging the piston over time, but this can considerably impair the astrometric precision. Another difficulty is Earth rotation, which implies that the baseline $\vec{B}$ changes between the two measurements. This is not a difficulty *per se*, because the effect of Earth rotation can be precisely estimated. However, the relative optical path difference $\overrightarrow{B(t_1)}\cdot\vec{\alpha} - \overrightarrow{B(t_2)}\cdot\vec{\beta}$ can be huge, and can introduce considerable biases because of errors in baseline estimation, atmospheric dispersion, etc. This also makes it a challenge to achieve high precision astrometry.

3.2. *Single field astrometry*

In the single field mode, or imaging mode, the interferometer detects simultaneously two objects, which are both in its field of view. In this case, the interference fringes are superposed. The measured quantity is a coherent flux **C** which is the sum of the coherent fluxes of the 2 objects:

$$\mathbf{C} = S_\alpha \exp\left(2\pi j \frac{\vec{B}\cdot\vec{\alpha}}{\lambda} + jP_{\rm atm}\right) + S_\beta \exp\left(2\pi j \frac{\vec{B}\cdot\vec{\beta}}{\lambda} + jP_{\rm atm}\right), \quad (7)$$

or

$$\mathbf{C} = \left[S_\alpha \exp\left(2\pi j \frac{\vec{B}\cdot\vec{\alpha}}{\lambda} + jP_{\rm atm}\right)\right]\left[1 + \frac{S_\beta}{S_\alpha}\exp\left(2\pi j \frac{\vec{B}\cdot(\vec{\beta}-\vec{\alpha})}{\lambda}\right)\right], \quad (8)$$

where S_α and S_β are the amplitudes of the two coherent fluxes (from the star and planet for example).

The techniques to obtain $\delta{\rm OPD} = \vec{B}\cdot(\vec{\beta}-\vec{\alpha})$ are multiple. One can look at the amplitude of the visibility $|\mathbf{C}|$ which changes as a function of $\vec{B}/\lambda$. Another technique uses the differential phase, i.e. the phase of **C** as a function of λ: one fits the modulation term $[1 + S_\beta/S_\alpha \exp(2\pi j(\vec{B}\cdot(\vec{\beta}-\vec{\alpha}))/\lambda)]$. Yet another technique computes the closure phase, and thereby removes the phase term in $[S_\alpha \exp(2\pi j(\vec{B}\cdot\vec{\alpha})/\lambda + jP_{\rm atm})]$.

Single field astrometry is widely used and efficient for a number of astronomical targets, but it is not practical for exoplanets. The main reason is that it mixes the flux of the planet and the star. The dynamic range is thus limited by the noise from the many stellar photons. In addition, biases limit the accuracy of phase measurements to half a degree. While an exoplanet, with a flux 10^{-4} fainter than its star, produces a signal of $360/10^4 = 0.036°$. Hence, single field astrometry doesn't reach the required precision on phase measurements to detect planets in high contrast systems.

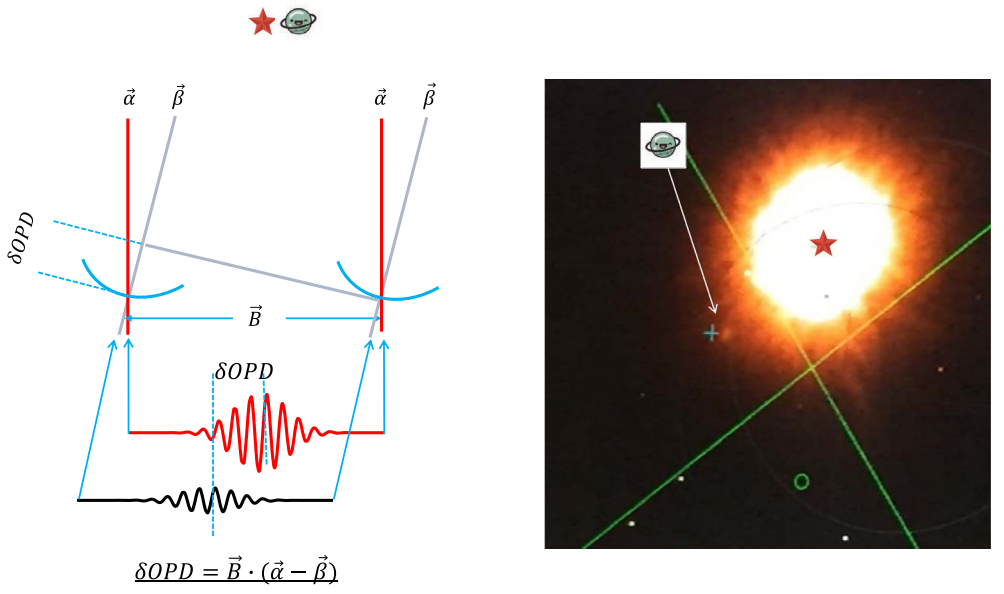

Figure 1. The principle of dual field interferometric astrometry. Right panel: acquisition camera of GRAVITY, with the wide field divided into two. The white arrow shows the position of the planet. Left panel: The planet and the star are simultaneously observed by 2 interferometers, one centered on the planet, the other on the star. Both interferometers detect a fringe pattern. The relative position of these two fringe patterns—also called relative optical path difference—is related to the scalar product of the separation between star ($\vec{\alpha}$) and planet ($\vec{\beta}$) times the baseline vector ($\vec{B}$). Thus the position of the planet relative to its star is precisely assessed from the relative location of the fringe patterns.

3.3. *Dual field astrometry*

In double field mode, the interferometer is in fact composed of two interferometers: one observes the star, the other observes the planet. The interferometer which observes the star usually acquires frames at high frequency in order to track the fringes, and hence to cancel the fast atmospheric perturbations. The second interferometer observes the fainter companion and acquires frames with long integration times. This minimizes the detector readout noise which could otherwise prevent the observation of faint objects. In the following, parameters that relate to the first, resp. second interferometer contain a subscript *FT*, resp. SCIENCE.

Each interferometer has a narrow field of view, typically of the size of the diffraction limit of a single telescope. With GRAVITY, the interferometers use single-mode fibers with acceptance cones equivalent to a field of view of 60 mas on the UTs. The right panel of Figure 1 shows the field of view of the GRAVITY acquisition camera, on which the 2 objects, the star and the companion, can be seen. The acquisition field of view is of the order of 2 arcseconds with the UTs. Within this small field, the interferometer selects an even smaller field of view, of the size of a point spread function (≈60 mas on the UTs). Therefore, both interferometers observe different astronomical objects. The first interferometer, points towards $\vec{\alpha}$ and measures a coherent flux equal to:

$$\mathbf{C_{FT}} = S_\alpha \exp\left(2\pi j \frac{\vec{B}\cdot\vec{\alpha}}{\lambda} + jP_{\rm atm}\right), \tag{9}$$

while the second interferometer, points towards $\vec{\beta}$ and measures a different coherent flux:

$$\mathbf{C_{SCIENCE}} = S_\beta \exp\left(2\pi j \frac{\vec{B}\cdot\vec{\beta}}{\lambda} + jP_{\rm atm} + j\mathrm{NCP}\right). \tag{10}$$

Precise metrology is necessary to measure the non-common optical path between the two interferometers (the NCP term). The relative optical path difference, $\vec{B}\cdot(\vec{\beta}-\vec{\alpha})$, can be deduced from a combination of the complex vectors:

$$\arg(\mathbf{C_{SCIENCE}}\cdot\mathbf{C_{FT}^*}\cdot\exp(-j\mathrm{NCP})) = 2\pi\frac{\vec{B}\cdot(\vec{\beta}-\vec{\alpha})}{\lambda}\ \%\ (2\pi). \tag{11}$$

For exoplanets, however, the situation is a little bit more complicated since the coherent flux on the science interferometer is often contaminated by the stellar flux (see reduction technique in Section 4).

The direct observation of exoplanets uses the double field mode. This mode is particularly interesting for several reasons. First, one interferometer precisely measures the phase of the star, and uses this to correct for atmospheric disturbances. This allows to freeze the turbulence on the second interferometer which observes the exoplanet. In that way, the second interferometer can make very long exposures on the exoplanet, with integration times above 100 s. Second, the science interferometer uses a single mode fiber which has the capacity to filter out the stellar light. This drastically attenuates the photon noise caused by the star on the science channel. These two effects have allowed to observe faint exoplanets with K magnitudes as large as 19, next to bright stars with K magnitudes down to 5.

4. Data reduction and stellar light removal

Despite our best efforts, on exoplanets at small angular separation, most of the flux that enters the science interferometer is still stellar light. This stellar light contributes to the detected signal in two ways. The dominant contribution is incoherent light: photons with phases that vary over milliseconds due to atmospheric perturbations. Over the long integration times (>10 s), the fringes of such atmospheric speckles are smeared out. This contribution is therefore denoted "incoherent flux". The second contribution comes from quasi-static speckles and is mostly due to imperfect optics: the phases of the associated photons are constant over several seconds, and produce coherent flux. This is a contribution from "coherent flux".

The plot in Figure 2 traces the two contributions as a function of the angular separation to the star. The three dashed lines represent the expected stellar flux observed as function of the performance of the adaptive optical (AO) correction, and as a function of the distance to the star. This is the flux that we expect to record in the science channel, the channel which is used to observe the exoplanet. The doted points are actual measurements. These measurements are observations of the exoplanetary system HD 95086, taken during technical time in the night of 14th February 2019.[1] The dotted blue points are the raw incoherent flux values recorded on the science detector. They roughly follow the prediction given by the red dashed line. The orange dots show the amount of coherent flux, that is the stellar flux which produces fringes, after leaking into the offset fiber of the science channel. Figure 2 shows that the coherent flux from the exoplanet is much smaller than the coherent flux from the star.

The exoplanet HD 95086 b [6] was observed at a separation of 624 mas. The contrast ratio between the planet and its star is 1.6×10^{-5}: the planet is a factor 62,500 fainter than the star. The flux leaked by the star into the science fiber is reduced by a factor 500, and is thus still 125

[1] ESO program ID 60.A-9102(A).

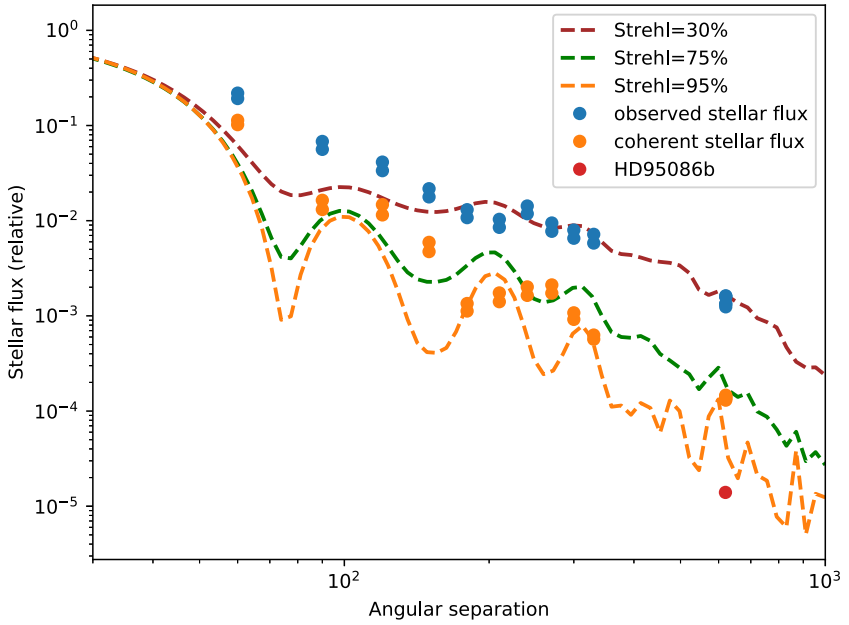

Figure 2. Incoherent (blue dots) and coherent (orange dots) flux as a function of angular separation, normalized by the total stellar flux, observed on HD 95086. The dashed curves are theoretical predictions of the incoherent flux as a function of the performance of the adaptive optical correction. The red dot shows the amount of coherent flux coming from the exoplanet HD 95086 b.

times brighter than the exoplanet. The coherent stellar flux is 12 times brighter than that of the exoplanet. So the key is to disentangle the coherent energies from the star and the exoplanet.

This is possible because the coherent energies from the star and the exoplanet have different phases. The observing procedure actually consists of two steps. In the first step, GRAVITY observes the star in both interferometers:

$$\mathbf{C_{FT}}(t_1) = S_{\rm star} \exp\left(2\pi j \frac{\vec{B}\cdot\vec{\alpha}}{\lambda}\right) \cdot \exp(jP_{t_1}) \tag{12}$$

$$\mathbf{C_{SCIENCE}}(t_1) = S_{\rm star} \exp\left(2\pi j \frac{\vec{B}\cdot\vec{\alpha}}{\lambda}\right) \cdot \exp(jP_{t_1} + j\mathrm{NCP}_{t_1}). \tag{13}$$

In a second step, the fringe tracker and science interferometer respectively observe the star and the exoplanet:

$$\mathbf{C_{FT}}(t_2) = S_{\rm star} \exp\left(2\pi j \frac{\vec{B}\cdot\vec{\alpha}}{\lambda}\right) \cdot \exp(jP_{t_2}) \tag{14}$$

$$\mathbf{C_{SCIENCE}}(t_2) = \left[S_{\rm planet} \exp\left(2\pi j \frac{\vec{B}\cdot\vec{\beta}}{\lambda}\right) + \mathbf{U_\lambda} \cdot S_{\rm star} \exp\left(2\pi j \frac{\vec{B}\cdot\vec{\alpha}}{\lambda}\right)\right] \cdot \exp(jP_{t_2} + j\mathrm{NCP}_{t_2}). \tag{15}$$

$\mathbf{U_\lambda}$ is the complex extinction caused by the off-axis pointing of the single mode fiber. In the case of HD 95086 b in Figure 2, $|\mathbf{U_\lambda}| \approx 1/5000$. But still, $S_{\rm planet} \approx 1/12 \times |\mathbf{U_\lambda}| \cdot S_{\rm star}$.

The goal is to derive $\vec{\alpha\beta} = \vec{\beta} - \vec{\alpha}$. To do so, we assume the following:

- we know $S_{\rm planet}/S_{\rm star}$ to a constant, ρ, which is the contrast ratio between the star and the planet.

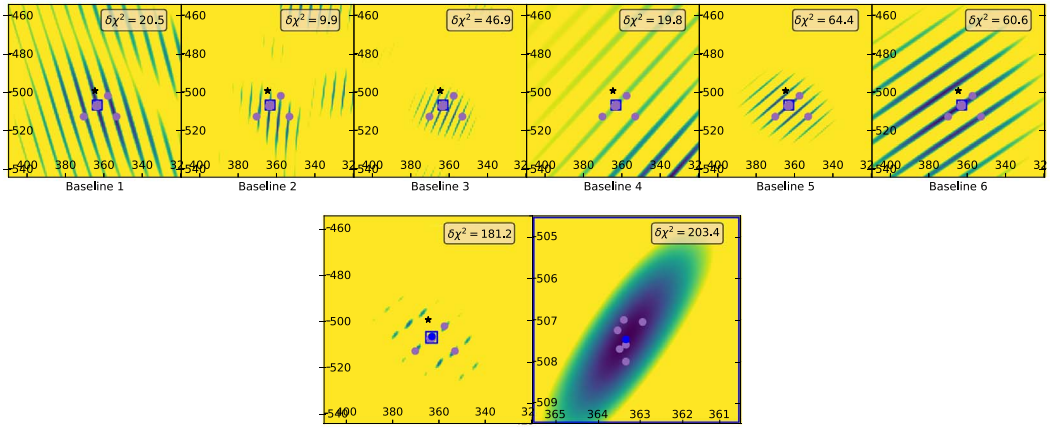

Figure 3. Search for the exoplanet in the HD95087 b data. The exoplanet is found by making a χ^2 map, as a function of $\overrightarrow{\alpha\beta}$ and minimized over the terms ρ and $\mathbf{u_{i,dit,baseline}}$. The 6 upper maps correspond to the χ^2 for a given pair of telescopes. The lower maps correspond to the generalized χ^2 map, with 2 different ranges for $\overrightarrow{\alpha\beta}$. The purple dots correspond to the minima for the 8 individual exposures. The scatter of the purple dots in the narrow $\overrightarrow{\alpha\beta}$ is used for computing the final error bars.

- $\mathbf{U_\lambda}$ is actually a polynomial as a function of lambda: $\mathbf{U_\lambda} = \sum_{i=0}^{N} \mathbf{u_{i,dit,baseline}} \lambda^i$. Where $\mathbf{u_{i,dit,baseline}}$ is a complex value which depends on the exposure time and baseline. The typical order of the polynomial is either $N = 4$ for large separations (>200 mas) or 6 for smaller separations.

So that we can estimate $\widetilde{\mathbf{C}}_{\mathbf{SCIENCE}}(t_2)$ from the equation:

$$\widetilde{\mathbf{C}}_{\mathbf{SCIENCE}}(t_2) = \frac{\mathbf{C_{FT}}(t_2)\cdot\mathbf{C_{SCIENCE}}(t_1)\exp(-j\mathrm{NCP}_{t_1})}{\mathbf{C_{FT}}(t_1)\exp(-j\mathrm{NCP}_{t_2})}\left[\rho\exp\left(2\pi j\frac{\overrightarrow{B}\cdot\overrightarrow{\alpha\beta}}{\lambda}\right)+\sum_{i=0}^{N}(\mathbf{u_{i,dit,baseline}})\lambda^i\right]. \tag{16}$$

The least square solution can then be calculated, over the full dataset, obtained for various wavelengths, integration times and baselines:

$$\chi^2 = \sum_{\lambda,\mathrm{dit},\mathrm{baseline}}\left|\frac{\mathbf{C_{SCIENCE}}-\widetilde{\mathbf{C}}_{\mathbf{SCIENCE}}}{\sigma_{\lambda,\mathrm{dit},\mathrm{baseline}}}\right|^2. \tag{17}$$

$\mathbf{C_{SCIENCE}}$ in Equation (16) is linear as a function of ρ and $\mathbf{u_{i,dit,baseline}}$. Hence a fast weighted linear regression can be used to find the minimum χ^2 for a given $\overrightarrow{\alpha\beta}$. Therefore, the data reduction consists in producing 2 dimensional χ^2 maps as a function of the right ascension and declination of $\overrightarrow{\alpha\beta}$.

The χ^2 maps obtained on the HD 95086 b dataset are shown in Figure 3. The data acquired on the exoplanet is made of 3 exposures, with 16 DITs of 30 s, with the 2 polarisations. Each polarisation was analysed separately, resulting into 6 data cubes. For each data cubes, the position of the minimum χ^2 is estimated (purple dots in Figure 2). It is interesting to see the multiple minima in the χ^2 maps, which can correspond to real detections, but with an error of 10 mas in the detected position. These minima reflect the fact that each baseline yields a degenerated answer in the right ascension and declination space. The four upper plots correspond to the χ^2 maps, minimized over the linear parameters ρ and $\mathbf{u_{i,dit,baseline}}$ for a single baseline. We can see that for a given pair of telescopes, the measurements are constrained

mostly along one axis, modulo a 2π in phase. The degeneracy can be seen to be caused by the term $\exp(2\pi j(\vec{B}\cdot\vec{\alpha\beta})/\lambda)$. The uncertainty on the scalar product, which causes the uncertainty perpendicularly to the baseline, disappears as Earth rotates. The uncertainty on the 2π term along the direction of the baseline can be reduced by increasing the width of the spectral bandpass.

The estimation of the error bars are obtained from the scatter of the χ^2 minimum in a reduced χ^2 map (purple dots in the lower right panel of Figure 2). The position of the exoplanet relative to its star is this way estimated to be 363.25 ± 0.09 mas in right ascension, and $-507,47 \pm 0.16$ mas in declination. An extra term is calculated, which is the covariance factor between the two directions. This value, also called Pearson correlation coefficient, is -0.31 in our dataset. The anti-correlation between right ascension and declination can be visualized by the χ^2 valley in the lower right panel of Figure 2.

5. Astrometric biases

5.1. *Biases caused by the baselines*

It is crucial to have an accurate estimate of the interferometric baseline $\vec{B}$. Indeed, as can be seen in Equation (4) an error on $\vec{B}$ translates directly into a bias on the measurement of $\vec{\beta}-\vec{\alpha}$. There are however at least 3 ways to define the interferometric baseline [7], as showed in Figure 4:

$\overrightarrow{B_{\rm WAB}}$: the vector joining the pivot points of the telescopes. This baseline does not change with the pointing of the telescopes. For this reason, it is often called the wide angle baseline, and used for wide angle mode observations.

$\overrightarrow{B_{\rm IMG}}$: the vector joining the telescopes' pupil centers. The definition of the pupil as the place where all beams cross independantly of their origin, makes this definition of the baseline independent of where the object lies in the field of the interferometer. It is therefore used to observe multiple objects in the field of a single interferometer, and when doing imaging astrometry.

$\overrightarrow{B_{\rm NAB}}$: the vector joining the positions of the metrological receivers. This baselines is useful when metrology is used to measure non common path values. It has the property of not changing whatever the path of the metrological light inside the interferometer. This baseline is used in dual field astrometry.

In a perfect interferometer the three vectors, corresponding to these three definitions, have the same length and direction. If this is the case, then the baseline is independent of the pointing direction of the telescope, of the position of the object in the interferometric field, and of the position of the optical metrology receivers. Unfortunately, no interferometer is perfect, and the three vectors are never strictly identical. An astrometric error budget has been established for GRAVITY followed by a three-step approach:

(1) A campaign to measure the pivot points of all telescopes in the Earth reference frame, using an external metrology system. The coordinates of these pivot points in the celestial reference system are obtained using the Earth Orientation Parameters given by the International Earth Rotation Service (IERS).
(2) To stabilize the telescope pupils, 4 beacons were installed on the spiders of the 4 telescopes. These beacons send light through the optical delay lines to the acquisition camera of the GRAVITY instrument. The beacons are used to stabilize the pupil of the instrument with a precision of 4 cm.
(3) The measurement points of the metrology system consist of 4 InGaAS photodetectors per telescope, placed on the spider arms. These detectors sense light sent from the recombination lab and that passes all optics of the interferometer up to M1, included.

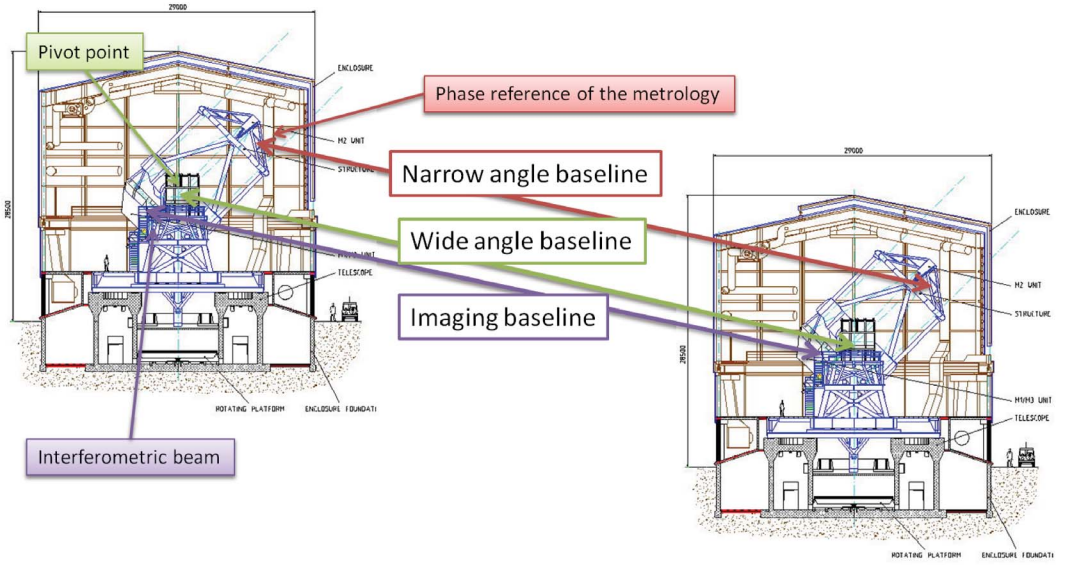

Figure 4. The 3 baselines of optical interferometry for astrometry: the wide angle baseline, the narrow angle baseline, and the imaging baseline.

The exact positions of these receivers were measured with respect to the pivot points of the telescope with an accuracy below the millimeter level. (Figure 4).

A more precise definition of these baselines, including mathematical definitions, is presented in [7] and [8]. According to theoretical investigations, and thanks to mitigation techniques, the bias introduced by inaccuracies in baseline estimations should still allow astrometric precisions of 10 μas in dual field observations.

5.2. *Other biases*

Inaccuracies in baseline estimations are the major source of bias. However, a few other biases were identified during GRAVITY operations. Most of them are related to non-common optical paths. They are of two types: the NCP which are not seen via metrology, and the NCP that are incorrectly seen through metrology.

Optical field aberrations are part of the first category. They especially affect single field imaging observations, where the objects are seen within the field of a single interferometer. These aberrations introduce a field-dependent phase offset, up to several tens of degrees. In single field observations, this NCP can be calibrated using a phase map [9]. However, in dual field interferometry, each target is maintained in the center of the field of each interferometer, so this effect is not a problem.

Dispersion is also part of the first category of undetected NCP. Up to the telescope entrance, the dispersion is caused by the atmosphere and is mostly identical between telescopes, so it cancels out and can be neglected. However, inside GRAVITY, if the differential delay lines between the fringe tracker and the science are not in vacuum, they introduce non-common-path dispersion. The GRAVITY differential delay lines are fiber-based and introduce a lot of dispersion. The solution used by GRAVITY is to probe the NCP with a laser which is at a wavelength close to the astrophysical light, at 1.9 μm. In addition, the remaining dispersion between the K band and 1.9 μm is estimated by the pipeline and added to the measure from the metrology.

High order aberrations are part of the second category of wrongly sensed NCP. The photodetectors used for metrology sample a small part of the pupil. High order aberrations are therefore sensed inaccurately, with errors up to 10° (60 nm). A solution consists in averaging these aberrations over time. Other mitigation techniques are currently developed by the GRAVITY collaboration in the context of GRAVITY+. GRAVITY+ is an ongoing effort to enhance the sensitivity of GRAVITY [10].

6. Some results and perspectives

6.1. *Astrometry of multi-planetary systems*

Following the first direct detection of an exoplanet by GRAVITY [11], the ExoGRAVITY team[2] started a campaign to survey a set of directly imaged exoplanets. At the beginning of the project, the only imaged multi-planetary system was HR 8799 [12]. PDS 70 c followed in 2019 with a detection in Hα by the MUSE instrument [13].

Around the same time, radial velocity campaigns started to hint at new planets that were young enough, and had long enough periods to be imaged. Lagrange *et al.* obtained evidence of a second planet in the β Pictoris system [14]. With a semi major axis of ≈ 2.7 AUs, it is closer to the star than β Pictoris b. GRAVITY observed it a few years later, using predictions on its position from radial velocity data [15, 16].

The HD 206893 system also happened to be very interesting. The presence of a brown dwarf orbiting at 10 AU was already known [17], but new HARPS data revealed the presence of another orbiting body, which appeared to be an exoplanet [18]. By combining radial velocity measurements, proper anomaly measurements from Gaia, and the GRAVITY astrometry of HD 206893 B, the on-sky position of HD 206893 c could be predicted in 2021 [19]. It was effectively detected, and characterized as a 12.7 ± 1 Mjup exoplanet, a year later by GRAVITY [20].

The astrometric accuracy of these observations shows that a few observations already constrain well the orbital parameters (Figure 5). For PDS70 b and c, two observations separated by 6 months allowed to derive the semi-major axis (20 ± 1 for b and 33.2 ± 2.5 for c). The eccentricity could also be established to 0.22 ± 0.07 and $0.05^{+0.05}_{-0.03}$ [21], under the assumption that the 2 exoplanets are co-planar. This assumption will be tested and verified with a few additional observations over the coming years.

For the Beta Pictoris system, the 2 planets were shown to be likely in a 7:1 mean motion resonance. The eccentricities of b and c were constrained to respectively 0.103 ± 0.003 and 0.32 ± 0.02. As for PDS 70, the inner companion has a higher eccentricity. Simulations show that the eccentricity of b can be explained by a transfer of momentum from c. This, in turn, could mean that b migrated inward, while preserving some of its eccentricity. It was also possible to observe the imprint of the 3 years orbital motion of b, on the astrometry of c! This gave a fully independent measurement of the dynamical mass of PDS 70 c: 10.4 ± 0.3 Mjup compared to the prior estimate of 8.89 ± 0.75 Mjup that includes radial velocity data [24].

6.2. *Prospects of improvement*

Astrometry with optical interferometers is currently limited to 10 to 100 μas, depending on the brightness of the source. In the context of the implementation of GRAVITY+ [10], several ameliorations are currently implemented to increase the accuracy of the astrometry of exoplanets. For faint planets the astrometry is limited by the faintness of the signal (like HD95086 b).

[2] ESO program ID 1104.C-0651.

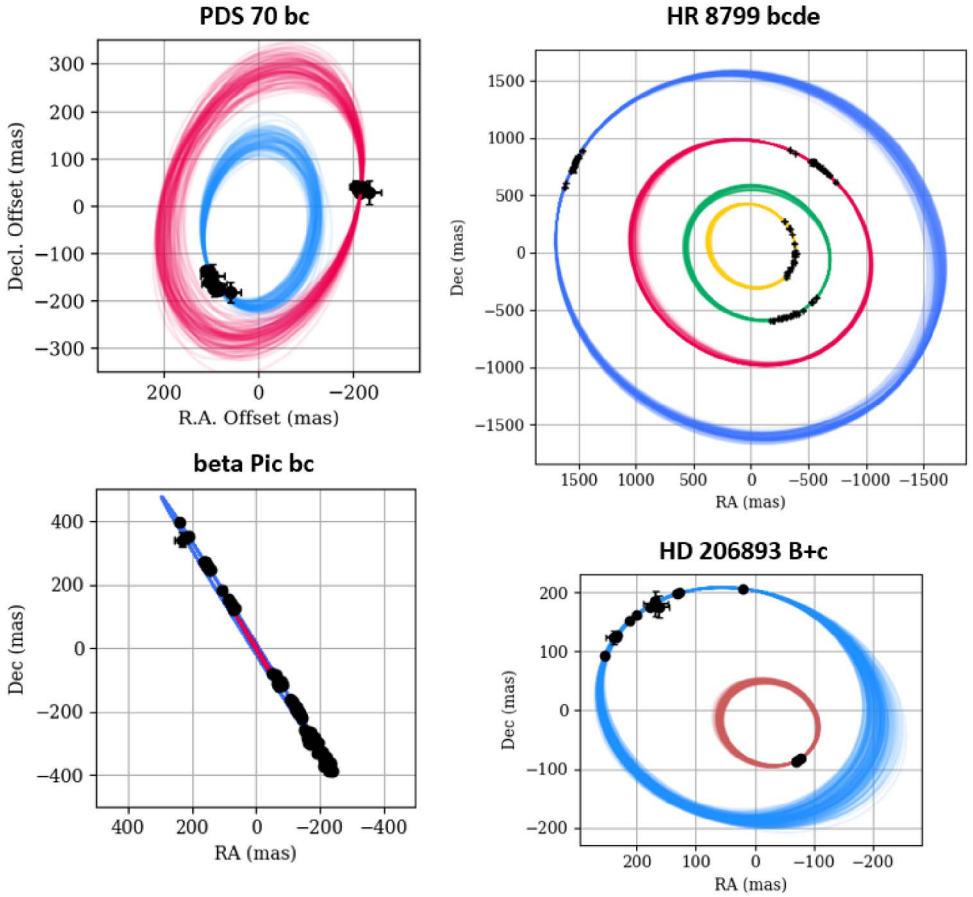

Figure 5. The four multi-planetary systems observed by the ExoGRAVITY large program [22]. The sizes of the systems are quite different, with parallaxes of 8.8, 24.2, 51, and 24.5 mas for PDS 70, HR 8799, Beta Pictoris, and HD 206893 respectively. It was possible to predict the orbital parameters (period, eccentricity) quite accurately, with only a few GRAVITY astrometric measurements, covering less than 3 years of orbital motion. The orbital trajectories were adjusted using the Orbitize! software [23].

Therefore, the goal of GRAVITY+ is to (i) decrease the photon noise caused by the incoherent stellar contamination and (ii) increase the planetary flux injected into the fiber. This will be achieved thank to a new adaptive optics correction which will reach high Strehl levels (green and orange dashed line in Figure 2). Another path taken is to improve the fringe tracking, to increase the contrast of the fringes and therefore the signal. For brighter object, a lot of work is on-going behind the scene to remove the last astrometric biases described in Section 5.

Another solution for the future is to increase the angular resolution of the optical interferometer. This can be done by observing exoplanets at shorter wavelengths. The VLTI transmit the flux down to a wavelength $\lambda = 1$ µm, so observing at this wavelength would give a factor 2 in accuracy compared to 2.2 µm. But a thrilling new project would be to build a new interferometer. This would allow to increase significantly $\vec{B}$. Such interferometer could also be optimised for visible wavelength. It could allow to resolve the exoplanets themselves, directly look for planetary companions, rings ...

Conflicts of interest

The author has no conflict of interest to declare.

Acknowledgements

Firstly, I would like to express my deep gratitude to the entire team that contributed to the development of the GRAVITY instrument. Without their tireless efforts and dedication, this project would not have been possible. Secondly, I extend my sincere appreciation to the members of the ExoGRAVITY team, whose contributions were instrumental in enabling us to make these groundbreaking exoplanetary observations. Additionally, I would like to thank Anthony Boccaletti and Aglae Kellerer for their invaluable assistance in proofreading this paper. Lastly, I am grateful for the support of the French ANR, which provided funding for this project through the grant Project-ANR-21-CE31-0017.

References

[1] A. Kellerer, "Beating the diffraction limit in astronomy via quantum cloning", *Astron. Astrophys.* **561** (2014), article no. A118.

[2] GRAVITY Collaboration, R. Abuter, M. Accardo, A. Amorim *et al.*, "First light for GRAVITY: Phase referencing optical interferometry for the very large telescope interferometer", *Astron. Astrophys.* **602** (2017), article no. A94.

[3] Gaia Collaboration, T. Prusti, J. H. J. de Bruijne, A. G. A. Brown *et al.*, "The Gaia mission", *Astron. Astrophys.* **595** (2016), article no. A1.

[4] J. T. Armstrong, D. Mozurkewich, L. J. Rickard *et al.*, "The navy prototype optical interferometer", *Astrophys. J.* **496** (1998), no. 1, p. 550-571.

[5] J. R. North, P. G. Tuthill, W. J. Tango, J. Davis, "γ^2 Velorum: orbital solution and fundamental parameter determination with SUSI", *Mon. Notices Royal Astron. Soc.* **377** (2007), no. 1, p. 415-424.

[6] J. Rameau, G. Chauvin, A.-M. Lagrange *et al.*, "Discovery of a probable 4-5 jupiter-mass exoplanet to HD 95086 by direct imaging", *Astrophys. J. Lett.* **772** (2013), no. 2, article no. L15.

[7] J. Woillez, S. Lacour, "Wide-angle, narrow-angle, and imaging baselines of optical long-baseline interferometers", *Astrophys. J.* **764** (2013), no. 1, article no. 109.

[8] S. Lacour, F. Eisenhauer, S. Gillessen *et al.*, "Reaching micro-arcsecond astrometry with long baseline optical interferometry. Application to the GRAVITY instrument", *Astron. Astrophys.* **567** (2014), article no. A75.

[9] GRAVITY Collaboration, R. Abuter, A. Amorim, M. Bauböck *et al.*, "Improved GRAVITY astrometric accuracy from modeling optical aberrations", *Astron. Astrophys.* **647** (2021), article no. A59.

[10] F. Eisenhauer, "GRAVITY+: Towards faint science", in *The Very Large Telescope in 2030, ESO Garching, Germany*, 2019, p. 30.

[11] GRAVITY Collaboration, S. Lacour, M. Nowak, J. Wang *et al.*, "First direct detection of an exoplanet by optical interferometry. Astrometry and K-band spectroscopy of HR 8799 e", *Astron. Astrophys.* **623** (2019), article no. L11.

[12] C. Marois, B. Zuckerman, Q. M. Konopacky, B. Macintosh, T. Barman, "Images of a fourth planet orbiting HR 8799", *Nature* **468** (2010), no. 7327, p. 1080-1083.

[13] S. Y. Haffert, A. J. Bohn, J. de Boer *et al.*, "Two accreting protoplanets around the young star PDS 70", *Nat. Astron.* **3** (2019), p. 749-754.

[14] A.-M. Lagrange, N. Meunier, P. Rubini *et al.*, "Evidence for an additional planet in the β Pictoris system", *Nat. Astron.* **3** (2019), p. 1135-1142.

[15] A. M. Lagrange, P. Rubini, M. Nowak *et al.*, "Unveiling the β Pictoris system, coupling high contrast imaging, interferometric, and radial velocity data", *Astron. Astrophys.* **642** (2020), article no. A18.

[16] M. Nowak, S. Lacour, A.-M. Lagrange *et al.*, "Direct confirmation of the radial-velocity planet β Pictoris c", *Astron. Astrophys.* **642** (2020), article no. L2.

[17] J. Milli, P. Hibon, V. Christiaens *et al.*, "Discovery of a low-mass companion inside the debris ring surrounding the F5V star HD 206893", *Astron. Astrophys.* **597** (2017), article no. L2.

[18] A. Grandjean, A.-M. Lagrange, H. Beust *et al.*, "Constraining the properties of HD 206893 B. A combination of radial velocity, direct imaging, and astrometry data", *Astron. Astrophys.* **627** (2019), article no. L9.

[19] J. Kammerer, S. Lacour, T. Stolker *et al.*, "GRAVITY K-band spectroscopy of HD 206893 B. Brown dwarf or exoplanet", *Astron. Astrophys.* **652** (2021), article no. A57.

[20] S. Hinkley, S. Lacour, G.-D. Marleau *et al.*, "Direct discovery of the inner exoplanet in the HD206893 system", *Astron. Astrophys.* **671** (2023), article no. L5.

[21] J. J. Wang, A. Vigan, S. Lacour *et al.*, "Constraining the nature of the PDS 70 protoplanets with VLTI/GRAVITY", *Astron. J.* **161** (2021), no. 3, article no. 148.

[22] S. Lacour, J. J. Wang, M. Nowak *et al.*, "The ExoGRAVITY project: using single mode interferometry to characterize exoplanets", in *Society of Photo-Optical Instrumentation Engineers (SPIE) Conference Series*, Society of Photo-Optical Instrumentation Engineers (SPIE) Conference Series, vol. 11446, 2020, p. 1144600.

[23] S. Blunt, J. J. Wang, I. Angelo *et al.*, "orbitize!: A comprehensive orbit-fitting software package for the high-contrast imaging community", *Astron. J.* **159** (2020), no. 3, article no. 89.

[24] S. Lacour, J. J. Wang, L. Rodet *et al.*, "The mass of β Pictoris c from β Pictoris b orbital motion", *Astron. Astrophys.* **654** (2021), article no. L2.